Statistical Characteristics in the Spectrum of Whistler Waves Near the Diffusion Region of Dayside Magnetopause Reconnection

Y. Ren, L. Dai, C. Wang, W. Li, X. Tao, B. Lavraud, O. Le Contel

Geophysical Research Letters

RESEARCH LETTER
10.1029/2020GL090816

Key Points:

- Whistler waves are mostly in a band around half the electron cyclotron frequency (Ω_e) on the magnetosphere side of reconnection
- Whistler waves are mainly below 1/2 Ω_e and peaked around 0.2 Ω_e on the magnetosheath side of reconnection
- A large part of the whistler waves events occurs in $T_{e\perp}/T_{e\parallel} < 1$ on the magnetosheath side of reconnection

Supporting Information:

- Supporting Information S1

Correspondence to:
L. Dai,
ldai@spaceweather.ac.cn

Citation:
Ren, Y., Dai, L., Wang, C., Li, W., Tao, X., Lavraud, B., & Le Contel, O. (2021). Statistical characteristics in the spectrum of whistler waves near the diffusion region of dayside magnetopause reconnection. *Geophysical Research Letters*, *48*, e2020GL090816. https://doi.org/10.1029/2020GL090816

Received 17 SEP 2020
Accepted 30 NOV 2020

Statistical Characteristics in the Spectrum of Whistler Waves Near the Diffusion Region of Dayside Magnetopause Reconnection

Y. Ren[1,2], L. Dai[1], C. Wang[1], W. Li[3], X. Tao[4], B. Lavraud[5], and O. Le Contel[6]

[1]State Key Laboratory of Space Weather, National Space Science Center, Chinese Academy of Sciences, Beijing, China, [2]University of Chinese Academy of Sciences, Beijing, China, [3]Center for Space Physics, Boston University, Boston, MA, USA, [4]Department of Geophysics and Planetary Sciences, CAS Key Laboratory of Geospace Environment, University of Science and Technology of China, Hefei, China, [5]Institut de Recherche en Astrophysique et Planétologie, Université de Toulouse, CNRS, UPS, CNES, Toulouse, France, [6]Laboratoire de Physique des Plasmas (LPP), CNRS/Ecole Polytechnique/Sorbonne Université/Université Paris-Saclay/Observatoire de Paris, Paris, France

Abstract Using Magnetospheric Multiscale (MMS) data, we present a statistical analysis revealing characteristics in the frequency spectrum of whistler waves in the vicinity of the diffusion region of magnetopause reconnection. On the magnetosphere side of reconnection, whistler waves are highly centered around the 1/2 electron cyclotron frequency (Ω_e). On the magnetosheath side of reconnection, whistler waves are mainly below 1/2 Ω_e and peaked around 0.2 Ω_e. The electron temperature anisotropy associated with the waves is evaluated. The occurrence rate of the whistler waves is large in the presence of perpendicular electron temperature anisotropy ($T_{e\perp}/T_{e\parallel} > 1$). However, a large part of the whistler waves events occurs in association with parallel electron temperature anisotropy ($T_{e\perp}/T_{e\parallel} < 1$) on the magnetosheath side of reconnection, reflecting a large number of the total observations with this electron condition. These results shed new lights on the whistler-related electron kinetic processes near the reconnection diffusion region.

Plain Language Summary Whistler waves are a type of electron-scale plasma waves that contribute to electron scattering, acceleration, and energy transport. Properties of whistler waves can provide diagnostic information on the electron kinetic-scale physics in magnetic reconnection. In this study, we use statistical data set from Magnetospheric Multiscale to characterize the spectral properties of whistler waves near magnetopause reconnection. Distinctive characteristics in the spectrum of whistler waves are found. On the magnetosphere side of reconnection, whistler waves are mostly in a band around half the electron cyclotron frequency. On the magnetosheath side of reconnection, whistler waves are mainly peaked around 0.2 electron cyclotron frequency. These statistical results of the spectral properties may shed light on whistler-related electron kinetic processes near reconnection diffusion region.

1. Introduction

Whistler waves are a type of electron-scale plasma waves that contribute to electron scattering, acceleration, and energy transport. Through wave-particle interactions, whistler waves shape the electron velocity distribution function. Properties of whistler waves can provide diagnostic information on the electron-scale physics in magnetic reconnection.

Whistler waves have been intensively studied in magnetic reconnection (e.g., Khotyaintsev et al., 2019). Cluster observations in the magnetotail show that whistler waves have been observed prior to and during reconnection (Wei et al., 2007). In magnetotail reconnection whistler waves are frequently observed near the separatrix region and the magnetic pileup region (S. Y. Huang et al., 2017). In the pileup region, free energy for whistler waves comes from the temperature anisotropy ($T_{e\perp}/T_{e\parallel} > 1$) that results from betatron heating (Fu et al., 2014; Fujimoto & Sydora, 2008; Khotyaintsev et al., 2011; Le Contel et al., 2009). Near the separatrix region of magnetotail reconnection, whistler waves are expected to be driven by field-aligned electron beams (Fujimoto, 2014; S. Y. Huang et al., 2016; Zhou et al., 2011). Analysis of Magnetospheric Multiscale (MMS) observations in magnetotail reconnection demonstrates that electron field-aligned crescent beams drive whistler waves through Landau resonance (Ren et al., 2019).

Electron populations are different on the two sides of magnetopause reconnection, with hot electrons on the magnetosphere side and relatively cold electrons on the magnetosheath side. As a result, whistler emissions and instabilities in magnetopause reconnection should differ from those in symmetric reconnection (Graham et al., 2016). Near the X-line of magnetopause reconnection, whistler waves have been observed in the vicinity of the electron diffusion region (EDR) (Burch et al., 2018; Cao et al., 2017; Tang et al., 2013). The most intense whistler waves are observed near the magnetosphere side separatrix region as revealed from Cluster observations (Graham et al., 2016) and recent MMS observations (J. Li et al., 2018; Le Contel et al., 2016; Khotyaintsev et al., 2020; Wilder et al., 2016, 2017, 2019; Yoo et al., 2018). Free energy for whistler waves in the magnetopause reconnection may originate from loss-cone electron distributions (Graham et al., 2016), perpendicular temperature anisotropy (Tang et al., 2013), and electron beams (Khotyaintsev et al., 2020; Wilder et al., 2017).

A general picture of the spectra of whistler waves in reconnection, however, has not yet been established from statistical data. By contrast, the spectral properties represent one of the most studied features of whistler waves in the context of radiation belt physics. According to the distinct characteristics in the wave spectrum, whistler-mode waves are categorized into hiss waves (with broadband and incoherent spectra) and chorus waves (with discrete and coherent spectra) (e.g., W. Li et al., 2012). In the frequency domain, Whistler-mode chorus waves often occur in the lower-band (0.1–0.5 Ω_e) and upper band (0.5–1 Ω_e) with a gap of wave power near 1/2 Ω_e (e.g., W. Li et al., 2012; Teng et al., 2019; Tsurutani & Smith, 1974). The nature of the whistler-mode chorus spectra, in particular the gap at 1/2 Ω_e, is still a puzzle to be conclusively resolved.

The aim of our study is to characterize the spectral properties of whistler waves near magnetopause reconnection. Statistical results of the spectral properties may shed light on whistler-related electron kinetic processes near reconnection diffusion region.

2. MMS Observations and Analysis

The data used in this study comes from instruments on MMS spacecraft (J. L. Burch, Moore, et al., 2016b). The DC magnetic field data is measured by fluxgate magnetometer (Russell et al., 2016). The 8192 Hz-sampling-rate magnetic field and electric field waveform data is provided by the search-coil magnetometer (SCM) (Le Contel et al., 2016b) and the electric field double probes (Ergun et al., 2016; Lindqvist et al., 2016). Plasma moments data (0.16 s cadence for ions and 0.03 s cadence for electrons) is from the fast plasma investigation (FPI; Pollock et al., 2016).

2.1. December 9, 2015 Event

Figure 1 shows MMS1 observations of the reconnection event on December 9, 2015. This reconnection event is selected as a representative case of the 29 reconnection events in the database. Figures 1a and 1b show the DC-low frequency magnetic field and ion velocity in the local normal boundary coordinate system. **L** is (0.20, −0.40, 0.89) GSM, **M** is (0.48, 0.84, 0.27) GSM, and **N** is (−0.86, 0.37, 0.36) GSM as determined from the minimum variance analysis of the magnetic field from 01:03 UT to 01:09 UT. The EDR (as marked by the shadow) was identified near 01:06:11 UT (Webster et al., 2018). Associated with V_{iL} reversal, the DC component of the B_N changes its direction near the X-line. These are classical signals of spacecraft crossing the X-line in the L direction (e.g., Burch et al., 2016b; Dai et al., 2011, 2015). The B_M shows monopolar structure during the crossing of the current layer. This signal is the Hall magnetic field and is consistent with kinetic Alfven wave eigenmode in asymmetric reconnection (Dai, 2009, 2018; Dai et al., 2017; H. Huang et al., 2018). The inferred trajectory of MMS is illustrated in Figure 1i. MMS enters the reconnection layer from the magnetosphere side, crosses the current sheet several times, passes the X-line, then leaves the reconnection layer and exits into the magnetosheath side.

The electron differential energy flux (DEF) data (Figure 1c) is smoothed over 0.3 s in time and over three energy bins. We categorize intervals based on the observed electron population. If a maximum value ($> 5{\cdot}10^6$ keVcm^{-2}sr^{-1}s^{-1} keV^{-1}) is detected in the electron DEF from 40 to 500 eV, the interval is recognized to have a magnetosheath electron population. In a similar manner, an interval is recognized to have a magnetosphere

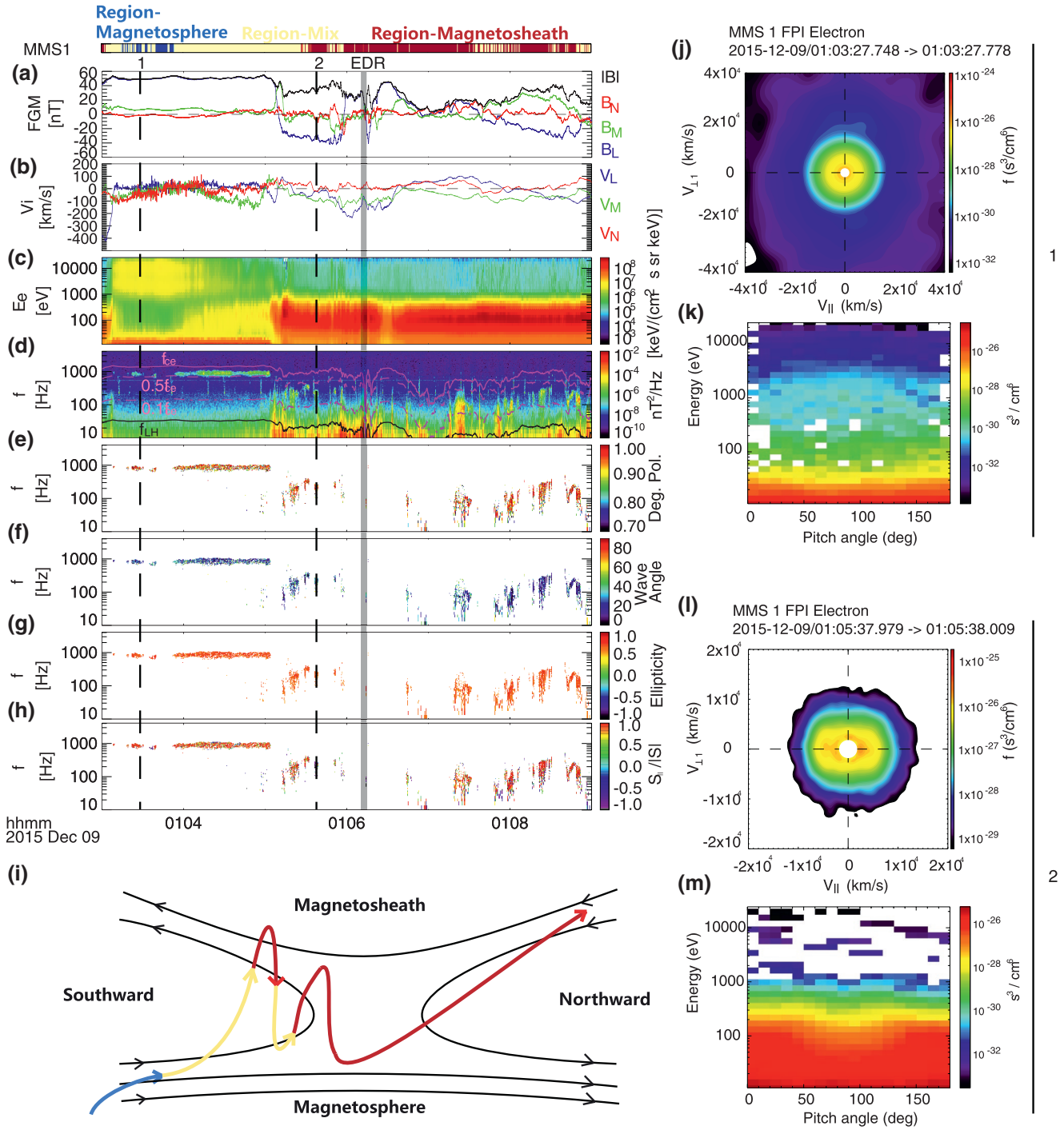

Figure 1. MMS1 observations on December 9, 2015 of dayside magnetopause reconnection region. (a) The magnetic field; (b) ion bulk flow velocity; (c) the electron omnidirectional differential energy fluxes; (d) the dynamic power spectra of magnetic field; (e) the degree of polarization; (f) the wave-normal angle; (g) the ellipticity; (h) the Poynting flux component along the background magnetic field; (i) the schematic of the MMS trajectory across this asymmetric reconnection region. (j, k) Electron 2-D velocity distribution and energy-pitch-angle distribution at 01:03:27 UT. (l, m) Electron 2-D velocity distribution and energy-pitch-angle distribution at 01:05:37 UT.

electron population if a maximum value larger than $3\cdot 10^5$ keVcm^{-2}sr^{-1}s^{-1} keV^{-1} is detected in electron DEF from 2 to 30 keV. The above threshold values for each category are based on typical values of electron flux in the magnetosphere (Baumjohann & Treumann, 1997) and the average profile of the 29 magnetopause

reconnection events in the database. The category of each interval is marked with bars of different color at the top of Figure 1. The list of 29 reconnection events with their category is enclosed in the supporting information.

Figures 1d–1h show the spectral properties of whistler waves. The dynamic spectra of the wave magnetic field are computed for sliding windows of 0.25 s-width with a time shift of 0.125 s between two continuous windows. Figures 1e–1h show the spectra of the degree of polarization, wave-normal angle (θ), ellipticity (Means, 1972; Samson & Olson, 1980), and the normalized Poynting flux in the parallel direction (Santolík et al., 2010). Whistler wave emission is identified with the following criteria. 1) The wave frequency is greater than lower hybrid frequency (f_{LH}) and less than electron cyclotron frequency (Ω_e). 2) The power spectral density (PSD) of the magnetic field is above the noise level (Hospodarsky, 2016). 3) The degree of polarization is greater than 0.7. 4) The ellipticity is greater than 0.5 (right-handed polarization with respect to **B**). 5) The bandwidth of the whistler emissions should be greater than 0.01 Ω_e and the duration larger than 0.25 s. The last criterion is to ensure that the identified signatures of whistler emissions are significant.

From 01:03 UT to 01:05 UT, structured bands of whistler waves near the frequency 1/2 Ω_e are observed in the regions of magnetosphere electrons and mixed electrons. The propagation of the observed whistler waves is toward the X-line (Figure 1h). These whistler mode waves have properties similar to those reported by previous MMS observation near the magnetosphere side of the separatrix (Graham et al., 2016; Le Contel et al., 2016; Wilder et al., 2017). In the region of magnetosheath electrons (after 01:05 UT), whistler waves are observed in the relatively broad frequency band below 1/2 Ω_e, with their field-aligned Poynting flux showing random distributions in both time and frequency domains (Figure 1h). The spectral feature of whistler waves on the magnetosheath side shows a similarity with the magnetosheath lion roars which have frequencies below a few hundred Hz and are usually observed together with local decreases in background magnetic field (Baumjohann et al., 1999; Giagkiozis et al., 2018). Consistent with this scenario, many intervals of magnetosheath whistler waves appear to be associated with local decrease in the magnetic field strength in Figure 1.

Representative electron distributions associated with whistler waves are shown. On the magnetosphere side (panels j–k), the electrons exhibit a loss-cone type distribution in the energy of 0.2–20 keV. On the magnetosheath side (panels l–m), the electron distribution appears to be stretched in the parallel and antiparallel direction in the energy of 50–200 eV.

2.2. Statistics of the Spectral Properties of Whistler Waves in Reconnection

We analyze the statistical properties of the spectra of whistler waves with the database consisting of the 29 magnetopause reconnection crossings of MMS during 2015–2016 as identified in Webster et al. (2018). Burst mode data of MMS1 within ±3 min near the EDR are selected for analysis. The criteria for identifying whistler waves are described in the case study. Each frequency bin in the identified whistler wave spectra is counted as one sample. The criteria yield 311,727 whistler samples in the spectra. The statistical properties of whistler wave spectra are summarized in Figures 2 and 3.

Figures 2a–2c show histogram distributions of whistler wave samples in the frequency spectra. Whistler-mode waves on the magnetosheath side of reconnection (Figure 2a) are mostly below 1/2 Ω_e. This feature is consistent with that in the case study of Graham et al. (2016). The occurrence of whistler waves sample's concentrates around the frequency 0.15–0.2 Ω_e. This pattern of frequency distribution is similar to that of whistler lion roars found in the magnetosheath (Giagkiozis et al., 2018). On the magnetosphere side of reconnection (Figure 2c), the distribution shows a strong concentration about the major peak 0.5–0.6 Ω_e. This feature is exactly opposite to that of whistler mode chorus showing a power gap at 1/2 Ω_e (Tsurutani & Smith, 1974). In addition to the major band near 1/2 Ω_e, a minor band of whistler waves around 0.1 Ω_e also appears on the magnetosphere side. We further check the phenomenon of the smaller peak around 0.1 Ω_e in individual reconnection events. Certain reconnection events (e.g., A8 and B31 in Webster et al. [2018]) indeed exhibit a band of whistlers around 0.1Ω_e in addition to the band 1/2 Ω_e on the magnetosphere side. In the region of mixed electrons (Figure 2b), spectra of whistlers wave events show two peaks near 0.15–0.2 and 1/2 Ω_e. This pattern in the mixed region is mostly the superposition of those on two sides of

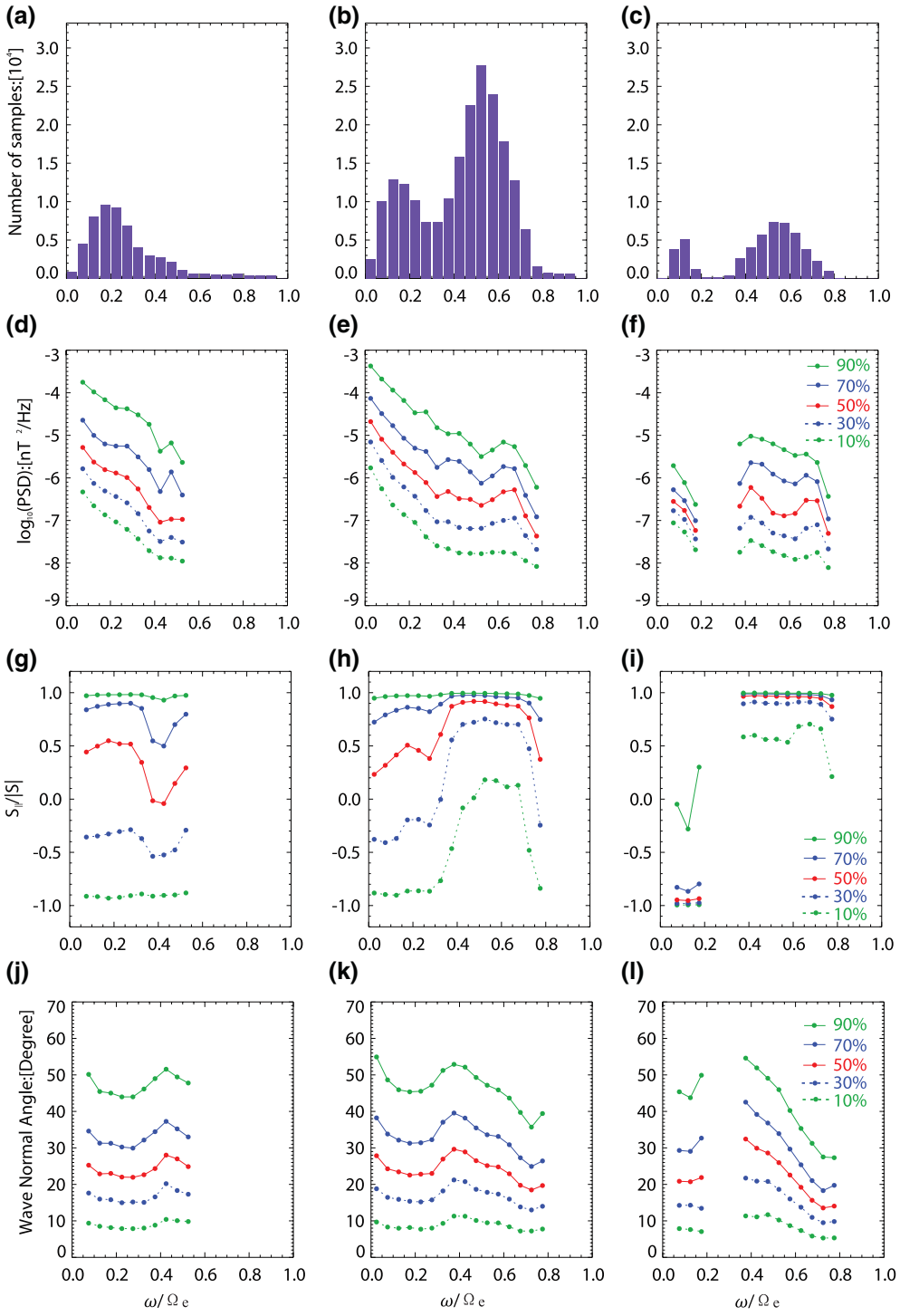

Figure 2. Statistic properties in the frequency spectra of whistler waves in different regions of reconnection. (a–c) The distribution of wave events on the frequency domain; (d–f) the power spectral density (PSD) distributions; (g–i) the parallel component of the Poynting flux spectral density; (j–l) the wave-normal angle (θ) distributions. The lines of the 10th percentile, 30th percentile, 50th percentile (Median value), 70th percentile, and 90th percentile of the data are shown.

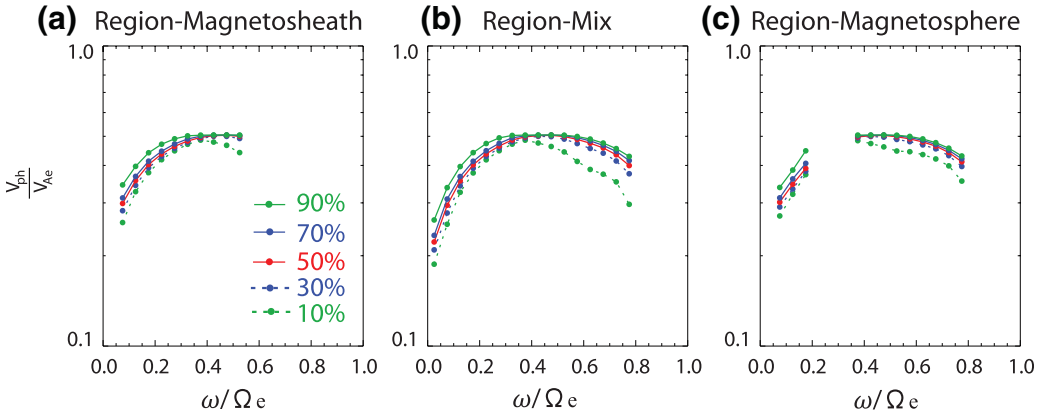

Figure 3. The spectra of the parallel propagation speed of whistler waves (normalized to the electron Alfven speed) based on the cold-plasma dispersion relation. The lines of the 10th percentile, 30th percentile, 50th percentile (Median value), 70th percentile, and 90th percentile of the data are shown.

reconnection. The two bands (near 0.2 and 1/2 Ω_e) of whistler waves usually do not co-exist at the same time in the region of mixed electrons, as noticed in examining individual reconnection events.

Figures 2d–2f show the PSD distributions of whistler waves in the frequency domain. We only plot data for frequency bins in which more than 1,000 samples occur. The lines of the 10th percentile, 30th percentile, 50th percentile (Median values), 70th percentile, and 90th percentile of the data are shown. The 10th percentile is equal to the value below which 10% of the observation data are to be found. On the magnetosheath side, the PSD of whistler waves decreases with frequency in the frequency band 0.1–0.5 Ω_e. The median value of the whistler PSD decreases by about 2 orders of magnitude from 10^{-5} nT^2/Hz to 10^{-7} nT^2/Hz in this frequency band. On the magnetosphere side, the median value of the whistler PSD is stable and around 10^{-7}–10^{-6} nT^2/Hz. In the region of mixed electrons, the PSD distribution behaves as a superposition of those on two sides of reconnection.

Figures 2g–2i are the spectra of the normalized field-aligned Poynting flux. On the magnetosheath side, the parallel Poynting flux of whistler waves near 0.2 Ω_e is equally distributed in the parallel and antiparallel directions. This feature is also shown in the December 9, 2015 event. On the magnetosphere side, the field-aligned Poynting flux around the peak of 1/2 Ω_e is mostly in the parallel direction. In contrast, the field-aligned Poynting flux around the peak of 0.1–0.15 Ω_e is mostly in the antiparallel direction. The two bands of whistler waves on the magnetosphere side of reconnection probably arise from a different source.

The spectra of the wave-normal angle of whistler waves are shown in Figures 2j–2l. Whistler waves on the magnetosheath side show a relatively even distribution of the wave-normal angle in the band below 1/2 Ω_e (Figure 2j). The range of the wave-normal angle is about 10–50 degrees, with the median value near 25°. On the magnetosphere side, the wave-normal angle of the main band near 1/2 Ω_e shows a decrease with the frequency, with a median value of 20°–35° and a range from 10 to 55 degrees. Whistler waves in both regions have a relatively broad range of wave-normal angle, suggesting that both cyclotron resonance and Landau resonance operate in the wave generation.

Figure 3 shows the spectra of the parallel propagation speed of whistler waves obtained from the cold-plasma dispersion relation, $c^2k^2 / \omega^2 = \omega_{pe}^2 / \omega(\Omega_e \cos\theta - \omega)$. Based on the parallel propagation speed, the minimum resonant energy of electrons can be roughly estimated from resonance condition $\omega - k_{||}v_{||} = n|\Omega_e|$ (W. Li et al., 2010; Thorne et al., 2005), where ω is the wave frequency, $k_{||}v_{||}$ is the parallel wave number multiplied by the particle parallel velocity, n is the resonance number. On the magnetosheath side, the median value of the parallel propagation speed for the band near 0.2 Ω_e is about 0.4 electron Alfven speed V_{Ae}. The corresponding resonance energy of electrons is 30 eV for the Landau resonance and 0.5–1.0 keV for the $n = \pm 1$ cyclotron resonance (assuming $\omega = 0.2\ \Omega_e$). On the magnetosphere side, the median value of the parallel propagation speed for the band near 1/2 Ω_e is about $0.5V_{Ae}$. The corresponding resonance energy of electrons is 10 keV for the Landau resonance and 10–100 keV for the $n = \pm 1$ cyclotron resonance (assuming

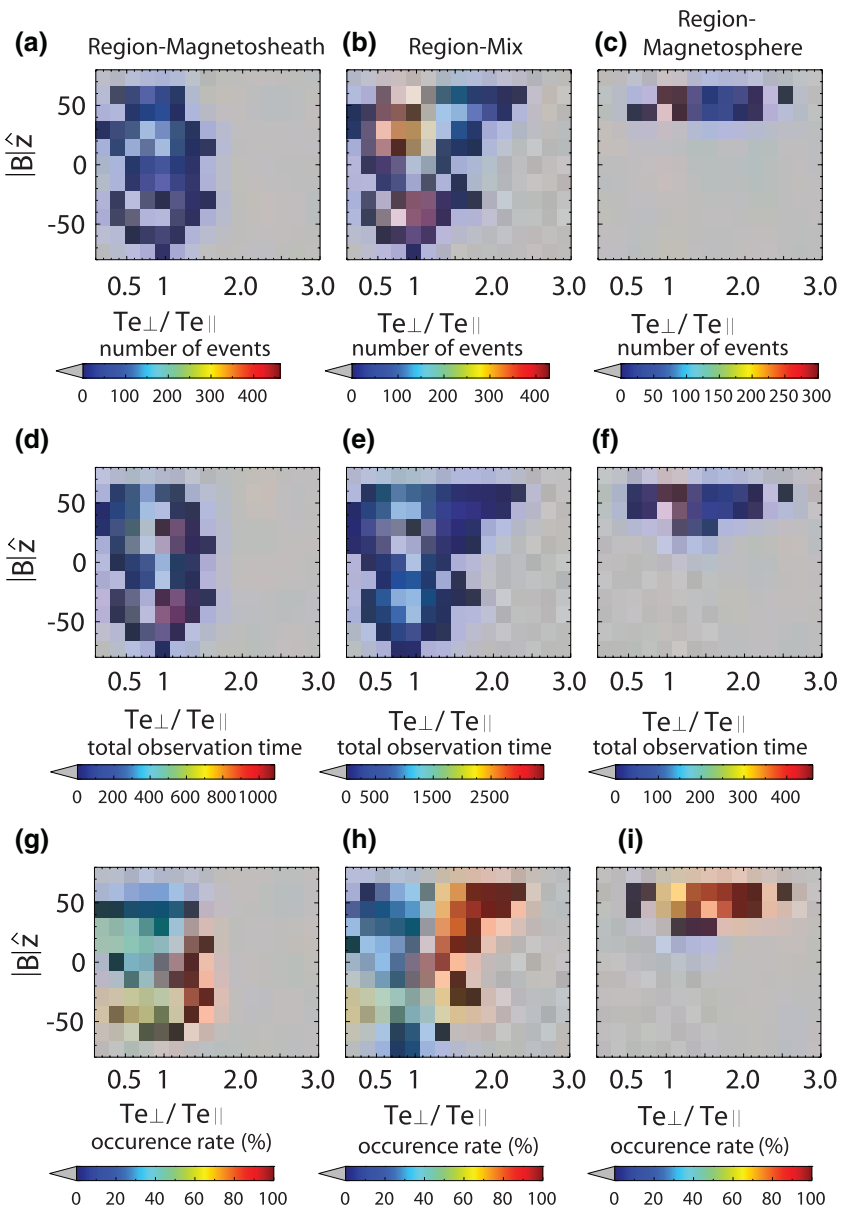

Figure 4. Distributions of the number of whistler events, the total observation time, and the occurrence rate of whistler waves as a function of the magnetic field and the ratio $T_{e\perp}/T_{e\|}$.

$\omega = 1/2\ \Omega_e$). The band near 0.1 Ω_e on the magnetosphere side has a smaller parallel velocity of $0.33V_{Ae}$. The typical resonance energy of electrons for the 0.1 Ω_e band is 6 keV for Landau resonance and 300–500 keV for $n = \pm 1$ cyclotron resonance (assuming $\omega = 0.1\ \Omega_e$). The estimated minimum resonance energy suggests different free energy source for whistler waves on two sides of reconnection.

2.3. Electron Temperature Anisotropy Associated With Waves

Figure 4 presents a survey of the electron temperature anisotropy $T_{e\perp}/T_{e\|}$ and the magnetic field (sign(B_z) $*|B|$) associated with the whistler waves. For the analysis in Figure 4, all the frequency band of whistler waves during one window (0.25 s) is counted as one event. Panels a–c show the number of whistler wave events, counted as the number of windows containing whistler waves. The total observation time (panels d–f) is counted as the number of all windows in observations. The occurrence rate (panels g–i) is the number of whistler wave events divided by the total observation time. On the magnetosheath side, whistler

waves are mostly associated with a parallel temperature anisotropy $T_{e\perp}/T_{e\parallel} \leq 1$ (panel a). By contrast, whistler waves on the magnetosphere side are mostly associated with a perpendicular temperature anisotropy $T_{e\perp}/T_{e\parallel} \geq 1$ (panel c). Panels d–f show that the temperature anisotropy of electrons generally is $T_{e\perp}/T_{e\parallel} \leq 1$ on the magnetosheath side and $T_{e\perp}/T_{e\parallel} \geq 1$ on the magnetosphere side. Panels g–i show the occurrence rate of the whistler wave event. In general, a high occurrence rate corresponds to perpendicular temperature anisotropy $T_{e\perp}/T_{e\parallel} \geq 1$ (with the median values of $T_{e\perp}/T_{e\parallel}$ at ∼1.14, ∼1.55, and ∼1.55 for occurrence rate larger than 80% in three regions, respectively), suggesting that perpendicular temperature anisotropy is an effective source of free energy in reconnection.

3. Summary and Discussion

We presented a statistical analysis of the spectral properties of whistler-mode waves in the vicinity of magnetopause reconnection. The database for the statistics consist of 29 magnetopause reconnection events that contain EDR as identified from MMS data during 2015–2016 by Webster et al. (2018). The main results of our study are as follows:

1. On the magnetosheath side of reconnection, whistler waves are concentrated below 1/2 Ω_e and peaked around 0.2 Ω_e in the frequency spectrum. This pattern in the spectra is consistent with that of magnetosheath lion roars (Baumjohann et al., 1999; Giagkiozis et al., 2018). The direction of the field-aligned Poynting flux of whistler waves is randomly distributed. Associated with the whistler waves, electron populations show a preference for a parallel temperature anisotropy ($T_{e\perp}/T_{e\parallel} < 1$).
2. On the magnetosphere side of reconnection, whistler waves are mostly centered around 1/2 Ω_e in the frequency spectrum. Occasionally, whistler waves exhibit a band near 0.1 Ω_e in addition to the major band 1/2 Ω_e. The field-aligned Poynting flux of the whistler waves is unidirectional. In particular, the directions of the field-aligned Poynting flux are opposite in the two bands near 1/2 Ω_e and 0.1 Ω_e. The electrons associated with whistler waves show a preference for a perpendicular temperature anisotropy ($T_{e\perp}/T_{e\parallel} \geq 1$).
3. In the region of mixed electrons from magnetosheath and magnetosphere, whistler wave spectra and corresponding electron anisotropy exhibit features that appear as a superposition of those from two sides. The two distinct types of whistler waves from magnetosheath and magnetosphere usually do not co-exist. In all regions, the wave-normal shows a broad distribution in the range of 10°–50°.

Whistler waves near magnetopause reconnection show distinct features in the frequency spectrum. Interestingly, the concentration of whistler power near 1/2 Ω_e is opposite to that of whistler waves showing a power gap near the 1/2 Ω_e in the inner magnetosphere. The concentration of whistler emissions near 1/2 Ω_e appear to be a puzzle that is of great interest for future investigations.

Our statistical results may shed light on the whistler wave generation and associated electron kinetic processes in magnetopause reconnection. On the magnetosphere side, the structured bands in the wave power and the unidirectional Poynting flux suggest that whistler waves are generated by coherent processes. Coherent free energy sources could be the loss-cone distribution as shown in Figures 1j–1k for the band near 1/2 Ω_e (Graham et al., 2016). Reconnection-accelerated magnetosheath electron beams (Khotyaintsev et al., 2020; Wilder et al., 2017) may be the source for the band near 0.1 Ω_e. The loss-cone distribution together with the reconnection-accelerated magnetosheath electron beam may form a Pacman distribution (Khotyaintsev et al., 2019). The loss-cone distribution may be a dominant contribution to the preference of perpendicular temperature anisotropy ($T_{e\perp}/T_{e\parallel} > 1$) as observed on the magnetosphere side. The loss-cone distribution generates whistler waves toward the X-line. The energy source may be local or come from a high-latitude **B** minima (Le Contel et al., 2016; Vaivads et al., 2007). The reconnection-accelerated magnetosheath electron beams generate whistler waves away from the X-line. The directions of the whistler waves in this scenario are consistent with the statistical results. The wave propagation as shown in Figure 2i may reflect that MMS was located in the southern magnetosphere for most EDR events in the database. The wave generation from the loss-cone distribution corresponds to the $n = \pm 1$ cyclotron resonance with magnetosphere electrons. The wave generation from reconnection-accelerated magnetosheath electrons corresponds to the $n = 0$ Landau resonance.

On the magnetosheath side, the field-aligned Poynting flux of whistler waves shows random distributions in the frequency and time domain, suggesting a mixed free energy source that are incoherent and probably

distributed over a broad region. Near the EDR, the magnetic field intensity decreases so that the electrons carry out the mirror motions and might result in the magnetosheath lion roars. The free energy could be 10–100 s eV magnetosheath electron field-aligned beams/crescent distributions as shown in Figure 1l–1m. Such electron distributions may correspond to a parallel temperature anisotropy ($T_{e\perp}/T_{e\parallel} < 1$) in the observations. The electron field-aligned beams/crescent are a natural product of magnetic reconnection (Burch et al., 2016b; Ren et al., 2019). MMS studies show that field-aligned electron beams are a common energy source for whistler waves (S. Huang et al., 2020; Ren et al., 2019; Zhao et al., 2020). In addition to the electron field-aligned beams, a fraction of whistler emissions may be also from 1 to 10 keV electrons that are accelerated in the pile up region on the magnetosheath side.

Data Availability Statement

The authors appreciate the MMS team and the MMS Science Data Center (https://lasp.colorado.edu/mms/sdc/public/) for providing the MMS data for this study.

Acknowledgments
This work at NSSC was supported by NNSFC grants (41874175, 41731070, 41674174, and 41631071), the Specialized Research Fund for State Key Laboratories of China, and the Strategic Pioneer Program on Space Science II, Chinese Academy of Sciences, grants XDA15350201, XDA15052500, and ZDEW-KT-2019-1. W. Li would like to acknowledge the Alfred P. Sloan Research Fellowship FG-2018-10936. The French involvement (SCM and FPI instruments) on MMS is supported by CNES and CNRS.

References

Baumjohann, W., & Treumann, R. A. (1997). *Basic space plasma physics*. World Scientific.
Baumjohann, W., Treumann, R. A., Georgescu, E., Haerendel, G., Fornacon, K. H., & Auster, U. (1999). Waveform and packet structure of lion roars. *Annales Geophysicae*, *17*(12), 1528–1534.
Burch, J. L., Moore, T. E., Torbert, R. B., & Giles, B. L. (2016a). Magnetospheric multiscale overview and science objectives. *Space Science Reviews*, *199*, 5–21.
Burch, J. L., Torbert, R. B., Phan, T. D., Chen, L., Moore, T. E., Ergun, R. E., et al. (2016b). Electron-scale measurements of magnetic reconnection in space. *Science*, *352*(6290), aaf2939.
Burch, J. L., Webster, J. M., Genestreti, K. J., Torbert, R. B., Giles, B. L., Fuselier, S. A., et al. (2018). Wave phenomena and beam-plasma interactions at the magnetopause reconnection region. *Journal of Geophysical Research: Space Physics*, *123*(2), 1118–1133. https://doi.org/10.1002/2017JA024789
Cao, D., Fu, H. S., Cao, J. B., Wang, T. Y., Graham, D. B., Chen, Z. Z., et al. (2017). MMS observations of whistler waves in electron diffusion region. *Geophysical Research Letters*, *44*(9), 3954–3962. https://doi.org/10.1002/2017GL072703
Dai, L. (2009). Collisionless magnetic reconnection via Alfvén eigenmodes. *Physical Review Letters*, *102*, 245. https://doi.org/10.1103/PhysRevLett.102.245003
Dai, L. (2018). Structures of hall fields in asymmetric magnetic reconnection. *Journal of Geophysical Research: Space Physics*, *123*(9), 7332–7341. https://doi.org/10.1029/2018JA025251
Dai, L., Wang, C., Angelopoulos, V., & Glassmeier, K. (2015). In situ evidence of breaking the ion frozen-in condition via the non-gyrotropic pressure effect in magnetic reconnection. *Annales Geophysicae*, *33*(9), 1147–1153.
Dai, L., Wang, C., Zhang, Y., Lavraud, B., Burch, J., Pollock, C., & Torbert, R. B. (2017). Kinetic Alfvén wave explanation of the hall fields in magnetic reconnection. *Geophysical Research Letters*, *44*(2), 634–640. https://doi.org/10.1002/2016GL071044
Dai, L., Wygant, J. R., Cattell, C. A., Dombeck, J. P., Thaller, S. A., Mouikis, C., et al. (2011). Cluster observations of surface waves in the ion jets from magnetotail reconnection. *Journal of Geophysical Research: Space Physics*, *116*(12), A12227. https://doi.org/10.1029/2011JA017004
Ergun, R. E., Tucker, S., Westfall, J. C., Goodrich, K. A., Malaspina, D. M., Summers, D., et al. (2016). The axial double probe and fields signal processing for the MMS mission. *Space Science Reviews*, *199*, 167–188.
Fu, H. S., Cao, J. B., Cully, C. M., Khotyaintsev, Y. V., Vaivads, A., Angelopoulos, V., et al. (2014). Whistler-mode waves inside flux pileup region: Structured or unstructured? *Journal of Geophysical Research: Space Physics*, *119*(11), 9089–9100. https://doi.org/10.1002/2014JA020204
Fujimoto, K. (2014). Wave activities in separatrix regions of magnetic reconnection. *Geophysical Research Letters*, *41*(8), 2721–2728. https://doi.org/10.1002/2014GL059893
Fujimoto, K., & Sydora, R. D. (2008). Whistler waves associated with magnetic reconnection. *Geophysical Research Letters*, *35*(19). https://doi.org/10.1029/2008GL035201
Giagkiozis, S., Wilson, L. B., Burch, J. L., Contel, O. L., Ergun, R. E., Gershman, D. J., et al. (2018). Statistical study of the properties of magnetosheath lion roars. *Journal of Geophysical Research: Space Physics*, *123*(7), 5435–5451. https://doi.org/10.1029/2018JA025343
Graham, D. B., Vaivads, A., Khotyaintsev, Y. V., & Andre, M. (2016). Whistler emission in the separatrix regions of asymmetric magnetic reconnection. *Journal of Geophysical Research: Space Physics*, *121*(3), 1934–1954. https://doi.org/10.1002/2015JA021239
Hospodarsky, G. B. (2016). Spaced-based search coil magnetometers. *Journal of Geophysical Research: Space Physics*, *121*, 12. https://doi.org/10.1002/2016JA022565
Huang, H., Yu, Y., Dai, L., & Wang, T. (2018). Kinetic Alfvén waves excited in two-dimensional magnetic reconnection. *Journal of Geophysical Research: Space Physics*, *123*(8), 6655–6669. https://doi.org/10.1029/2017JA025071
Huang, S., Xu, S., He, L., Jiang, K., Yuan, Z., Deng, X., et al. (2020). Excitation of whistler waves through the bidirectional field-aligned electron beams with electron temperature anisotropy: MMS observations. *Geophysical Research Letters*, *47*(14), e2020GL087515. https://doi.org/10.1029/2020GL087515
Huang, S. Y., Fu, H. S., Yuan, Z., Vaivads, A., Khotyaintsev, Y. V., Retino, A., et al. (2016). Two types of whistler waves in the hall reconnection region. *Journal of Geophysical Research: Space Physics*, *121*(7), 6639–6646. https://doi.org/10.1002/2016JA022650
Huang, S. Y., Yuan, Z., Sahraoui, F., Fu, H. S., Pang, Y., Zhou, M., et al. (2017). Occurrence rate of whistler waves in the magnetotail reconnection region. *Journal of Geophysical Research: Space Physics*, *122*(7), 7188–7196. https://doi.org/10.1002/2016JA023670
Khotyaintsev, Y. V., Cully, C. M., Vaivads, A., Andre, M., & Owen, C. J. (2011). Plasma jet braking: Energy dissipation and nonadiabatic electrons. *Physical Review Letters*, *106*(16), 165001.
Khotyaintsev, Y. V., Graham, D. B., Steinvall, K., Alm, L., Vaivads, A., Johlander, A., et al. (2020). Electron heating by Debye-scale turbulence in guide-field reconnection. *Physical Review Letters*, *124*(4), 145101.

Khotyaintsev, Y. V., Graham, D. B., Norgren, C., & Vaivads, A. (2019). Collisionless magnetic reconnection and waves: Progress review. *Frontiers in Astronomy and Space Sciences*, *6*. https://doi.org/10.3389/fspas.2019.00070

Le Contel, O., Retino, A., Breuillard, H., Mirioni, L., Robert, P., Chasapis, A., et al. (2016a). Whistler mode waves and hall fields detected by MMS during a dayside magnetopause crossing. *Geophysical Research Letters*, *43*(12), 5943–5952. https://doi.org/10.1002/2016GL068968

Le Contel, O., Roux, A., Jacquey, C., Robert, P., Berthomier, M., Chust, T., et al. (2009). Quasi-parallel whistler mode waves observed by themis during near-earth dipolarizations. *Annales Geophysicae*, *27*(6), 2259–2275. https://doi.org/10.5194/angeo-27-2259-2009

Le Contel, O., Leroy, P. L., Roux, A., Coillot, C., Alison, D., Bouabdellah, A., et al. (2016b). The search-coil magnetometer for MMS. *Space Science Reviews*, *199*, 257–282. https://doi.org/10.1007/s11214-014-0096-9

Li, J., Bortnik, J., An, X., Li, W., Russell, C. T., Zhou, M., et al. (2018). Local excitation of whistler mode waves and associated Langmuir waves at dayside reconnection regions. *Geophysical Research Letters*, *45*(17), 8793–8802. https://doi.org/10.1029/2018GL078287

Li, W., Thorne, R., Bortnik, J., Tao, X., & Angelopoulos, V. (2012). Characteristics of hiss-like and discrete whistler-mode emissions. *Geophysical Research Letters*, *39*(18). https://doi.org/10.1029/2012GL053206

Li, W., Thorne, R. M., Nishimura, Y., Bortnik, J., Angelopoulos, V., McFadden, J. P., et al. (2010). THEMIS analysis of observed equatorial electron distributions responsible for the chorus excitation. *Journal of Geophysical Research*, *115*(1), A00F11. https://doi.org/10.1029/2009JA014845

Lindqvist, P., Olsson, G. F., Torbert, R. B., King, B., Granoff, M., Rau, D., et al. (2016). The spin plane double probe electric field instrument for MMS. *Space Science Reviews*, *199*, 137–165.

Means, J. D. (1972). Use of the three dimensional covariance matrix in analyzing the polarization properties of plane waves. *Journal of Geophysical Research*, *77*(28), 5551–5559.

Pollock, C. J., Moore, T. E., Jacques, A., Burch, J. L., Gliese, U., Saito, Y., et al. (2016). Fast plasma investigation for magnetospheric multiscale. *Space Science Reviews*, *199*, 331–406.

Ren, Y., Dai, L., Li, W., Tao, X., Wang, C., Tang, B., et al. (2019). Whistler waves driven by field-aligned streaming electrons in the near-earth magnetotail reconnection. *Geophysical Research Letters*, *46*(10), 5045–5054. https://doi.org/10.1029/2019GL083283

Russell, C. T., Anderson, B. J., Baumjohann, W., Bromund, K. R., Dearborn, D., Fischer, D., et al. (2016). The magnetospheric multiscale magnetometers. *Space Science Reviews*, *199*, 189–256.

Samson, J. C., & Olson, J. V. (1980). Some comments on the descriptions of the polarization states of waves. *Geophysical Journal International*, *61*(1), 115–129.

Santolík, O., Pickett, J. S., Gurnett, D. A., Menietti, J. D., Tsurutani, B. T., & Verkhoglyadova, O. (2010). Survey of Poynting flux of whistler mode chorus in the outer zone. *Journal of Geophysical Research*, *115*, A00F13. https://doi.org/10.1029/2009JA014925

Tang, X., Cattell, C. A., Dombeck, J. P., Dai, L., Wilson, L. B., Breneman, A., & Hupach, A. (2013). THEMIS observations of the magnetopause electron diffusion region: Large amplitude waves and heated electrons. *Geophysical Research Letters*, *40*(12), 2884–2890. https://doi.org/10.1002/grl.50565

Teng, S., Tao, X., & Li, W. (2019). Typical characteristics of whistler mode waves categorized by their spectral properties using Van Allen probes observations. *Geophysical Research Letters*, *46*(7), 3607–3614. https://doi.org/10.1029/2019GL082161

Thorne, R. M., Horne, R. B., Glauert, S., Meredith, N. P., Shprits, Y. Y., Summers, D., & Anderson, R. R. (2005). The influence of wave-particle interactions on relativistic electron dynamics during storms. *Geophysical Monograph Series* (Vol. 159). American Geophysical Union.

Tsurutani, B. T., & Smith, E. J. (1974). Postmidnight chorus: A substorm phenomenon. *Journal of Geophysical Research*, *79*(1), 118–127.

Vaivads, A., Santolík, O., Stenberg, G., André, M., Owen, C., Canu, P., & Dunlop, M. (2007). Source of whistler emissions at the dayside magnetopause. *Geophysical Research Letters*, *34*(9), L09106. https://doi.org/10.1029/2006GL029195

Webster, J. M., Burch, J. L., Reiff, P. H., Daou, A. G., Genestreti, K. J., Graham, D. B., et al. (2018). Magnetospheric multiscale dayside reconnection electron diffusion region events. *Journal of Geophysical Research: Space Physics*, *123*(6), 4858–4878. https://doi.org/10.1029/2018JA025245

Wei, X. H., Cao, J. B., Zhou, G. C., Santolik, O., Reme, H., Dandouras, I., et al. (2007). Cluster observations of waves in the whistler frequency range associated with magnetic reconnection in the Earth's magnetotail. *Journal of Geophysical Research*, *112*, A10225. https://doi.org/10.1029/2006JA011771

Wilder, F. D., Ergun, R. E., Goodrich, K. A., Goldman, M. V., Newman, D. L., Malaspina, D. M., et al. (2016). Observations of whistler mode waves with nonlinear parallel electric fields near the dayside magnetic reconnection separatrix by the magnetospheric multiscale mission. *Geophysical Research Letters*, *43*(12), 5909–5917. https://doi.org/10.1002/2016GL069473

Wilder, F. D., Ergun, R. E., Hoilijoki, S., Webster, J. M., Argall, M. R., Ahmadi, N., et al. (2019). A survey of plasma waves appearing near dayside magnetopause electron diffusion region events. *Journal of Geophysical Research: Space Physics*, *124*(10), 7837–7849. https://doi.org/10.1029/2019JA027060

Wilder, F. D., Ergun, R. E., Newman, D. L., Goodrich, K. A., Trattner, K. J., Goldman, M. V., et al. (2017). The nonlinear behavior of whistler waves at the reconnecting dayside magnetopause as observed by the magnetospheric multiscale mission: A case study. *Journal of Geophysical Research: Space Physics*, *122*(5), 5487–5501. https://doi.org/10.1002/2017JA024062

Yoo, J., Jara-Almonte, J., Yerger, E., Wang, S., Qian, T., Le, A., et al. (2018). Whistler wave generation by anisotropic tail electrons during asymmetric magnetic reconnection in space and laboratory. *Geophysical Research Letters*, *45*(16), 8054–8061. https://doi.org/10.1029/2018GL079278

Zhao, D., Fu, S., Parks, G. K., Chen, L., Liu, X., Tong, Y., et al. (2020). Modulation of whistler mode waves by ion-scale waves observed in the distant magnetotail. *Journal of Geophysical Research: Space Physics*, *125*(2), e2019JA027278. https://doi.org/10.1029/2019JA027278

Zhou, M., Pang, Y., Deng, X. H., Yuan, Z., & Huang, S. Y. (2011). Density cavity in magnetic reconnection diffusion region in the presence of guide field. *Journal of Geophysical Research: Space Physics*, *116*, A06222. https://doi.org/10.1029/2010JA016324